OPEN ACCESS
IOP PUBLISHING
SCIENCE AND TECHNOLOGY OF ADVANCED MATERIALS
Sci. Technol. Adv. Mater. **14** (2013) 014401 (12pp)
doi:10.1088/1468-6996/14/1/014401

# Nanoscale structure and atomic disorder in the iron-based chalcogenides

**Naurang Lal Saini**

Dipartimento di Fisica, Università di Roma 'La Sapienza', Piazzale Aldo Moro 2, I-00185 Roma, Italy

E-mail: naurang.saini@roma1.infn.it

Received 15 November 2012
Accepted for publication 11 January 2013
Published 21 February 2013
Online at stacks.iop.org/STAM/14/014401

**Abstract**
The multiband iron-based superconductors have layered structure with a phase diagram characterized by a complex interplay of charge, spin and lattice excitations, with nanoscale atomic structure playing a key role in their fundamental electronic properties. In this paper, we briefly review nanoscale structure and atomic disorder in iron-based chalcogenide superconductors. We focus on the $Fe(Se,S)_{1-x}Te_x$ (11-type) and $K_{0.8}Fe_{1.6}Se_2$ (122-type) systems, discussing their local structure obtained by extended x-ray absorption fine structure. Local structure studies on the $Fe(Se,S)_{1-x}Te_x$ system reveal clear nanoscale phase separation characterized by coexisting components of different atomic configurations, similar to the case of random alloys. In fact, the Fe–Se/S and Fe–Te distances in the ternary $Fe(Se,S)_{1-x}Te_x$ are found to be closer to the respective distances in the binary FeSe/FeS and FeTe systems, showing significant divergence of the local structure from the average one. The observed features are characteristic of ternary random alloys, indicating breaking of the local symmetry in these materials. On the other hand, $K_{0.8}Fe_{1.6}Se_2$ is known for phase separation in an iron-vacancy ordered phase and an in-plane compressed lattice phase. The local structure of these 122-type chalcogenides shows that this system is characterized by a large local disorder. Indeed, the experiments suggest a nanoscale glassy phase in $K_{0.8}Fe_{1.6}Se_2$, with the superconductivity being similar to the granular materials. While the 11-type structure has no spacer layer, the 122-type structure contains intercalated atoms unlike the 1111-type REFeAsO (RE = rare earth) oxypnictides, having well-defined REO spacer layers. It is clear that the interlayer atomic correlations in these iron-based superconducting structures play an important role in structural stability as well as superconductivity and magnetism.

Keywords: local structure, 11-type chalcogenides, random alloys, phase separation, glassy phases

## 1. Introduction

Since the discovery of superconductivity more than 100 years ago, many diverse classes of superconducting materials have been found and subsequently studied in detail. However, an increasing number of emerging superconducting materials have been found to show many features that are inconsistent with the standard Bardeen–Cooper–Schrieffer (BCS) theory. The real problem lies in the complexity of the new superconductors unlike the conventional BCS superconductors. Indeed, recent years have seen that the physics of emerging superconductors should be lying in the diverse range of exotic magnetic, electronic and crystal structures, coexisting at different locations in the same crystal. Incidentally, the superconductivity is introduced by tuning indirectly the fundamental electronic structure, either by chemical substitution, intercalation and disorder or by varying external conditions. In all these, the structural topology of the material is changed, and the nanoscale structure is different from the one assumed to



 

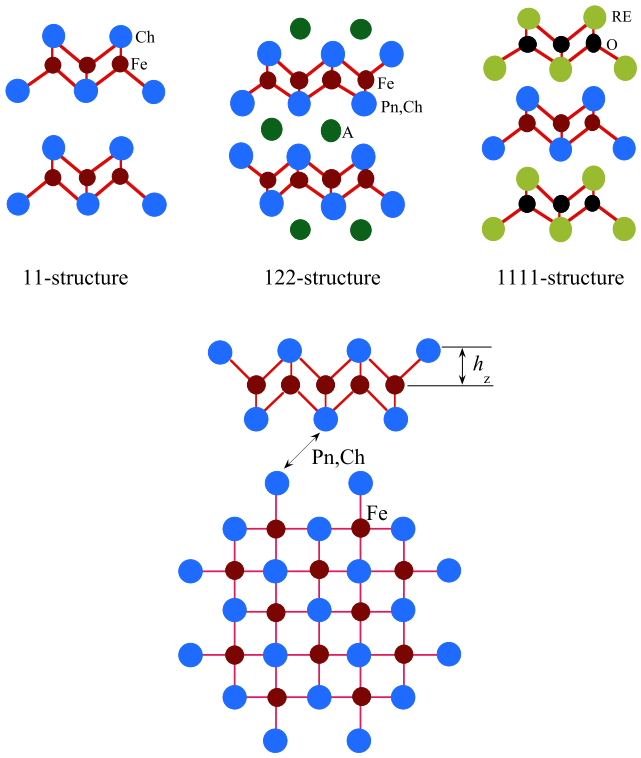


**Figure 1.** Crystal structure of 11-type, 122-type and 1111-type iron-based superconducting materials. These materials have layered structure with a common Fe-square plane (lower) and the presence or absence of a spacer layer with the Fe–Fe distance being ∼2.7 Å. The Fe atoms are tetrahedrally coordinated with pnictogen (Pn)/chalcogen (Ch) anions (at a distance of ∼2.4 Å) where the anion height $h_z$ is an important parameter for describing the fundamental electronic structure of these materials.

be described by first principle models. As the nanoscale structure is modified while tuning the fundamental electronic structure, understanding this nanoscale structure–macroscopic function relationship is at the heart of complex matter showing quantum phenomena such as superconductivity.

The recent discovery of superconductivity in iron-based layered structures [1] has created a great deal of interest and new hope to find more adaptable superconducting materials. Thanks to much effort, we know a series of new classes of layered iron-based superconducting structures [2–6]. Among these, the REOFeAs (RE = La, Ce, Pr, Nd, Sm) system has ZrCuSiAs-type parent structure and is now commonly called the '1111' system, while the $AFe_2As_2$ (A = Sr, Ba) system has $ThCr_2Si_2$-type parent structure and is called the '122' system. In addition, there are two other series, the so-called '111' LiFeAs system with PbFCl-type structure and the FeSe '11' system with PbO-type structure [2]. The crystal structure of 11-type, 122-type and 1111-type iron-based materials is shown in figure 1. Recently, more complicated structures were found to show superconductivity [10]. Common to all these structures is the Fe-square plane and the layered structure (see, e.g., figure 1). The maximum $T_c$ of 55 K is achieved in the 1111 system by electron or hole doping through F-substitution for O or by introducing oxygen defects. On the other hand, the 122-structures show a maximum $T_c$ of about 40 K, obtained by appropriate substitution of bivalent alkali cations with monovalent alkali metals (K, Cs, etc). The discovery of intercalated FeSe with 122-structure [11] has added further flavor to the already rich iron-based superconductivity research.

In a short time, by theoretical and experimental research through a large number of studies, it has been clarified that the iron-based materials are characterized by a phase diagram with the superconductivity appearing close to the antiferromagnetic ordering of the cuprates [2–5]. The electronic structure is made of several hole-like and electron-like Fermi surfaces derived by Fe 3d orbitals and their variable degeneracy [12–15]. The pressure and strain effects [16] play a vital role and the materials manifest coexisting phases characterized by different competing electronic degrees of freedom.

The coexistence of superconductivity with a complex magnetic structure seems to be related to the atomic correlations between the $FePn(Ch)_4$ (Pn = pnictogen and Ch = chalcogen) layer and spacer layers, making these materials very interesting, with correlating electronic degrees of freedom and multiscale functions. The multiple band electronic structure of these systems could lead to a significant change in the material functions due to intra- and inter-band pairing interactions and the degeneracy of different bands. Although the iron-based superconductors are quite different from the cuprates, they share common ingredients for the high-$T_c$ superconductivity. They are layered materials with multiband electronic structure and multiple Fermi surfaces controlled by the $Fe(Pn,Ch)_4$ tetrahedra (figure 1). One of the structural parameters regulating the Fermi surface of these materials is the 'anion height', i.e. the height of the anion from the Fe-square lattice planes [17, 18] (see, e.g., $h_z$ in figure 1). Indeed, by chemical substitutions or intercalations, the Fermi surface properties could be manipulated by changing the $h_z$ and hence the $T_c$. All these underline the importance of the structural topology and optimization of the local structure, having a direct correlation with the electronic structure and the novel quantum state of superconductivity in these materials.

The main experimental probes used to determine the local structure in the new iron-based superconductors are pair distribution function (PDF) analysis of x-ray and neutron diffraction, and extended x-ray absorption fine structure (EXAFS) [19–34]. The PDF is based on real space (Fourier transform (FT)) analysis of diffraction patterns measured up to high wave vectors, involving diffuse peaks due to atomic displacements, in addition to the main diffraction peaks, and hence is a probe of the local structure, providing information on the distribution of the atomic distances [35]. The most direct method for probing local structure is EXAFS, which is an atomic site-selective method, providing information on the local atomic distribution around a selected absorbing site through scattering of the photoelectron exited from the x-ray absorbing atom with the near neighbors [36]. Although the PDF and EXAFS techniques have their own limitations in determining quantitative atomic displacements, there is good agreement on the local lattice displacements determined by these techniques in complex materials [37–46]

including the new iron-based superconductors [19–34]. The contribution of EXAFS has been vital, owing to the availability of high-brilliance x-ray synchrotron radiation sources. In combination with recent technical advances and available high brilliance x-ray synchrotron radiation sources, EXAFS spectroscopy has allowed us to determine quantitative atomic displacements, offering a unique approach to pinpoint short-range atomic displacements and their dynamics, being a fast ($\sim 10^{-15}$ s) and local ($\sim$5–6 Å) probe [36].

Here, we have briefly reviewed important results on the local structure of iron-based chalcogenide superconductors. We have confined ourselves to studies of local structure by EXAFS, and cited related work wherever required in the text. The following section is dedicated to the basic concepts of EXAFS as a probe of local and instantaneous atomic displacements, describing salient features of the data analysis and experimental approach with relevant justification. We have restricted our focus to experimental results on the local structure of the active $FeCh_4$ layer, i.e. around the Ch and Fe atoms. We describe the characteristic local structure in the $Fe(Se,S)_{1-x}Te_x$ (11-type) chalcogenides and show that these materials are similar to random alloys with broken local symmetry. This is followed by a brief review on the local structure of the $K_{0.8}Fe_{1.6}Se_2$ (122-type) system, in which FeSe is interlated by K, showing a glassy nature. Finally, we provide a brief summary with relevant conclusions on the basis of local structure with respect to the electronic properties of these chalcogenides.

## 2. EXAFS as a probe of local structure

Before presenting results on the local structure of the iron-based chalcogenides, it is useful to provide a brief introduction to the EXAFS technique as a probe of local structure. The intrinsic time scale of the technique is given by the core–hole lifetime, $\sim 10^{-15}$ s, which is faster than the phonon lifetime ($\sim 10^{-12}$ s). Therefore, EXAFS is a fast tool for the study of local structure, probing not only static but also dynamic local displacements in a physical system. This is unlike diffraction techniques where an ordered structure is probed within a time scale of $\sim 10^{-9}$ s. The x-ray absorption coefficient $\mu(E)$ is generally given by the product of the matrix element times the joint density of states for the electronic transitions from the initial to final states (core–hole). It can be solved in real space for electronic transitions from an initial localized core level to a final state, described as an outgoing spherical wave that interferes with the waves backscattered from the neighboring atoms [36], i.e.

$$\mu(E) = \mu_0(E)\left[1 + \sum_{n\geqslant 2}\chi_n(E)\right], \tag{1}$$

where $\mu_0(E)$ is the so-called atomic absorption coefficient for the selected atomic core level and $\chi_n(E)$ represents the contribution arising from all multiple scattering pathways beginning and ending at the central absorbing atom and involving $(n-1)$ neighboring atoms. The modulation function (EXAFS oscillations) $\chi(E)$ can be extracted from the experimentally recorded absorption coefficient and is given as

$$\chi(E) = \sum_{n\geqslant 2}\chi_n(E) = \frac{\mu(E) - \mu_0(E)}{\mu_0(E)}. \tag{2}$$

The shortest scattering pathway is the one that involves the first shell $\chi_2(E)$ term being relevant. This term can be isolated from the $\chi_n(E)$ by Fourier filtering as all multiple scattering pathways that contribute to $\chi_n(E)$ with $n \geqslant 3$, as well as all contributions from further shells, have longer scattering path lengths. The single scattering EXAFS signal $\chi_2(k)$ for the first shell can be written as

$$\chi_2(k) = \sum_i \frac{S_0^2\, e^{-\frac{2R_i}{\lambda}}}{kR_i^2} A_i(k) e^{-2k^2\sigma_i^2} \sin[2kR_i + \delta_i(k)], \tag{3}$$

where $R_i$ is the radial distance for the first shell and $\delta_i(k)$ the phase function determined by both the photoabsorber and the nearest-neighbor backscattering atoms. The $S_0^2$ is an amplitude correction factor due to the photoelectron correlation and is also called the passive electron reduction factor. $A_i(k)$ is the scattering power, $\lambda$ is the photoelectron mean free path and $\sigma_i^2$ is the correlated Debye–Waller factor (DWF) of the photoabsorber–backscatter atom pairs. The scattering power is given by $A_i(k) = N_i^* F_i(k)$, where $N_i^*$ is the average coordination number and $F_i(k)$ is the backscattering amplitude of the neighboring atoms, and hence equation (3) takes the following form:

$$\chi_2(k) = \sum_i N_i^* \frac{S_0^2\, e^{-\frac{2R_i}{\lambda}}}{kR_i^2} F_i(k) e^{-2k^2\sigma_i^2} \sin[2kR_i + \delta_i(k)]. \tag{4}$$

Here the photoelectron wavevector ($k$ in Å$^{-1}$) is given by

$$k = \frac{p}{\hbar} = \frac{\sqrt{2m(E - E_0)}}{\hbar}, \tag{5}$$

where $E$ (eV) is the incident photon energy while $E_0$ (eV) is the ejected photoelectron energy origin. For the oriented samples, the EXAFS signal has a dependence on the angle between the preferred sample direction and the x-ray polarization vector. Therefore, the EXAFS equation can be generalized as

$$\chi(k) = \sum_i 3N_i \cos^2\theta_i \frac{S_0^2\, e^{-\frac{2R_i}{\lambda}}}{kR_i^2} F_i(k) e^{-2k^2\sigma_i^2} \sin[2kR_i + \delta_i(k)], \tag{6}$$

where $N_i$ is the equivalent number of neighboring atoms at a distance $R_i$ sitting at the angle $(\theta_i)$ with respect to the direction of the electric field of the polarized x-ray beam [36]. Therefore with the polarized light and single-crystal samples, the EXAFS could be exploited to obtain information on directional local structure.

The effect of temperature on the EXAFS signal is taken care of by the exponential term $\exp(-k^2\sigma_i^2)$. The $\sigma_i^2$ is the DWF of the absorber–scattering atom pair. The $\sigma_i^2$ appearing in the EXAFS equation is not the same as the one determined by the diffraction experiments. While the diffraction DWF measures mean-square deviation of

a given atom from its average site, the EXAFS DWF measures the mean square relative displacements (MSRD), determined by the correlated movement of the absorber and the scattering atoms. The EXAFS DWF $\sigma_i^2$ could be presented as a sum of a temperature-independent (static $\sigma_0^2$) and a temperature-dependent (dynamic $\sigma^2(T)$) term, i.e, the temperature-dependent part $\sigma^2(T)$ could be given by the simple correlated Einstein model as [47, 48]

$$\sigma^2(T) = \frac{\hbar^2}{2\mu k_B \theta_E} \coth \frac{\theta_E}{2T}, \tag{7}$$

where $\omega_E$ is the bond vibration frequency, $\mu$ is the reduced mass of the pair and $\theta_E = \hbar\omega_E / k_B$ is the Einstein temperature. Considering all the above facts, it is clear that the EXAFS DWF provides important information on the local atomic displacements and dynamics.

To extract the structural parameters from an EXAFS signal, the shift of the photoelectron energy origin $E_0$ and the phase shifts should be known [48, 52]. These parameters can be either fixed or allowed to vary when an experimental EXAFS is parameterized. For further details of the experiments and data analysis, see our earlier publications [22, 26, 28–31].

## 3. Results and discussion

### *3.1. Local structure of the 11-type structure: broken local symmetry and random alloy-like behavior*

Among the iron-based superconductors, FeSe (a 11-type chalcogenide) shows the lowest superconducting transition temperature ($T_c \sim 8\,K$); however, it could be considered a model system for addressing basic characteristics of these materials [7]. The FeSe structure contains simple stacking of tetrahedrally coordinated $FeSe_4$ layers (see, e.g., figure 1) without spacer layers that are known to have a substantial effect on the electronic properties [22, 23]. Substitution by Te in FeSe leads to a marginal increase in $T_c$ (∼15 K). For more on the general properties of 11-type superconductors, see reviews [7–9]. Here, we will start the discussion with a presentation of the local structure of the simplest iron-based superconductor, i.e. 11-type structure. The experiments on the local structure reveal that the iron chalcogenides with 11-structure are similar to random alloys [49]. Indeed, these materials show phase separation characterized by different iron–chalcogen bond lengths at the nanoscale.

Figure 2 shows an example of Se *K*-edge EXAFS oscillations on a binary FeSe and a ternary $FeSe_{0.5}Te_{0.5}$ system. The EXAFS oscillations show apparent differences in the local structure of binary and ternary systems. These differences can be appreciated better in the FT providing real-space information. Figure 3 shows FT magnitudes of the Se *K*-edge EXAFS oscillations at 200 K, not corrected for the photoelectron phase shifts, providing partial atomic distribution around the Se atoms. The structure of the 11-system has tetragonal symmetry at room temperature (figure 1). The FeSe shows a structural transition to an orthorhombic phase below ∼100 K [50, 51]. For the Se site

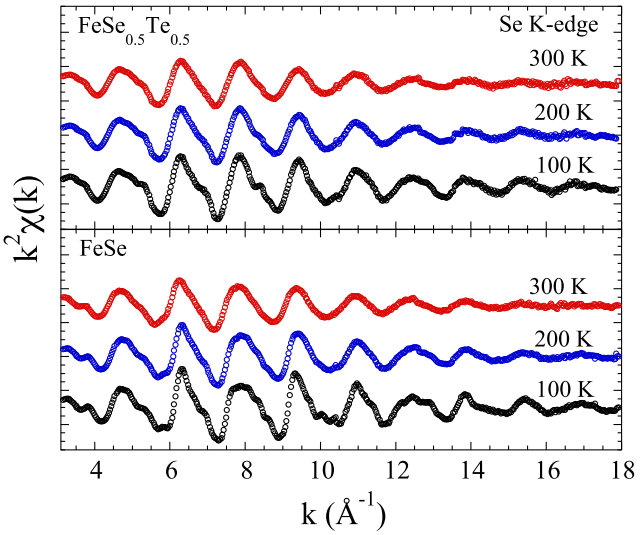


**Figure 2.** Se *K*-edge EXAFS on binary $FeSe_{0.88}$ and ternary $FeSe_{0.5}Te_{0.5}$ at several temperatures. Differences in the local structure of the binary and ternary systems are evident from the EXAFS oscillations.

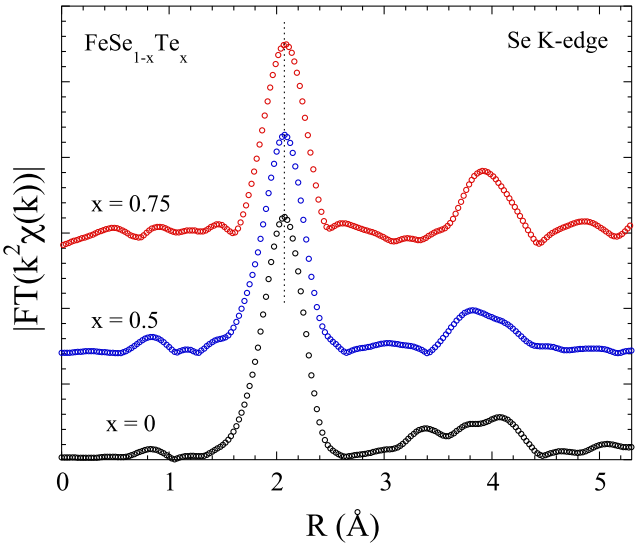


**Figure 3.** FT magnitudes of the Se *K*-edge EXAFS oscillations at 200 K, measured on the 11-system with different Te concentrations (not corrected for the photoelectron phase shifts). The position of the main peak due to Fe–Se distance hardly shows any change with Te substitution.

(probed by Se *K*-edge EXAFS), there are four Fe nearest neighbors at a distance of ∼2.4 Å (the main peak at ∼2 Å). The next nearest neighbors of Se are eight Se(Te) and four Fe atoms. Contributions of these distant shells appear mixed, giving a multiple structured peak at ∼3.0–4.5 Å. From the raw data it is clear that the position of the FT peak due to Fe–Se distance (the main FT peak) does not change with Te concentration, indicating that the Fe–Se distance in the $FeSe_{1-x}Te_x$ remains constant.

It is possible to analyze the EXAFS data using a model with a single Fe–Se distance extracting information on the distance and the related MSRD, determined by the correlated

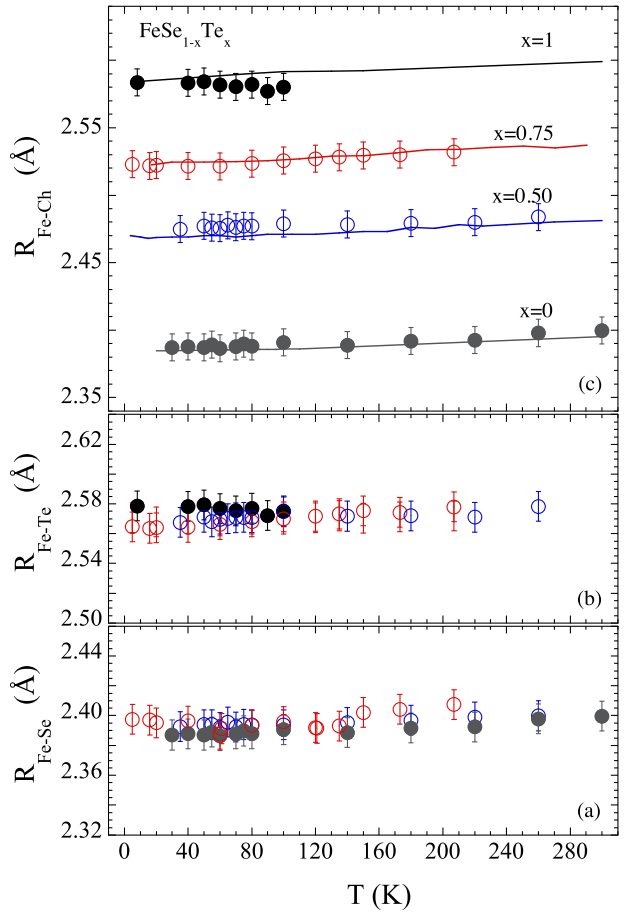


**Figure 4.** Fe–Se (a) and Fe–Te (b) distances in the $FeSe_{1-x}Te_x$ ($0 \leqslant x \leqslant 1$) samples as a function of temperature [26, 29]. The open symbols correspond to the ternary systems and the filled symbols are due to binary FeSe and FeTe. The Fe–Te (b) and Fe–Se (c) bond lengths in the $FeSe_{1-x}Te_x$ ternary are quite similar to those in the respective binary FeSe and FeTe. The local Fe–Ch distances measured by EXAFS (symbols) are compared with the average diffraction distances (solid lines) in panel (c) [50, 51].

DWFs ($\sigma^2$) [26]. The Fe–Se distances can be determined also by Fe *K*-edge EXAFS analysis [29]. Indeed, the nearest neighbors of Fe are Ch (Ch = Se, Te) atoms at a distance of ∼2.4 Å and the next Fe atoms at a distance of ∼2.7 Å. The Fe–Se distances measured by Fe *K*-edge EXAFS are similar to these determined by the Se *K*-edge EXAFS [26, 29], showing the importance of the use of EXAFS to study the local structure of these materials. Since the nearest neighbors of Fe are Se and Te atoms, the Fe *K*-edge EXAFS also permits one to measure the Fe–Te distance. Incidentally, EXAFS results on the Fe–Se and Fe–Te distances are similar both for polycrystalline [26, 29] and single-crystal [27] samples.

Figure 4 shows temperature dependence of the local bond lengths determined by EXAFS in samples with different Te concentrations. The Fe–Se and Fe–Te distances in the ternary $FeSe_{1-x}Te_x$ system are similar to the Fe–Se and Fe–Te distances in the binary FeSe and FeTe, respectively, showing hardly any change with temperature. It is clear from the results that the chalcogen atom locations in the ternary systems are significantly displaced from the average crystallographic sites,

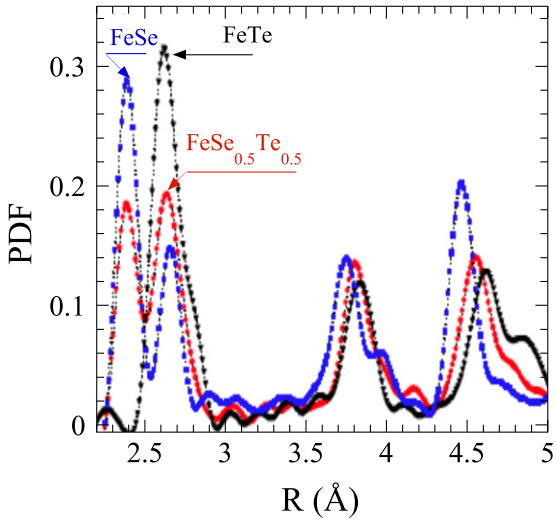


**Figure 5.** Local atomic structure of $FeSe_{1-x}Te_x$ studied by neutron PDF analysis [19]. PDF for three compositions (two binary systems, FeSe and FeTe, and the ternary $FeSe_{0.5}Te_{0.5}$ system) are shown, revealing that the local structure of the ternary $FeSe_{0.5}Te_{0.5}$ is characterized by different Fe–Ch bond lengths.

i.e. the crystal is composed of a mixture of well-defined long and short Fe–Ch bonds.

The local structure of the $FeSe_{1-x}Te_x$ system has also been investigated [19] by neutron diffraction PDF analysis. From a detailed analysis, the authors have extracted the bond lengths and bond angles, and found that the average structure of the $FeSe_{0.5}Te_{0.5}$ superconductor does not accurately represent the bond length and bond angles between Fe and the two chalcogens. Indeed, locally, the Se and Te ions do not share the same site and have two distinct *z*-coordinates, in contrast to what is presumed in the crystallographic average tetragonal symmetry. For ready reference, the local atomic structure of three compositions (two binary systems, FeSe and FeTe, and the ternary $FeSe_{0.5}Te_{0.5}$ system) described by PDF [19] is shown in figure 5. In the FeSe, the first two peaks correspond to the shortest distances in the tetrahedral unit, i.e. the Fe–Se and the Fe–Fe bond lengths. The wide peak with a right shoulder in the binary FeTe is due to the contributions from Fe–Te and Fe–Fe nearest neighbor distances as the separation between Fe–Fe and Fe–Te is not well resolved. On the other hand, the two peaks in the ternary $FeSe_{0.5}Te_{0.5}$ system are due to Fe–Se and Fe–Te (mixed with Fe–Fe) distances. Figure 5 clearly shows that the Fe–Se and Fe–Te distances in the ternary system are similar to the Fe–Se distance in the binary FeSe and the Fe–Te distance in the binary FeTe system. This is similar to what has been observed by EXAFS analysis on the $FeSe_{1-x}Te_x$ system. It is worth mentioning that local structure studies revealing nanoscale phase separation are consistent with the phase separation observed by tunneling experiments on the $FeSe_{1-x}Te_x$ system [53, 54].

Not only in the $FeSe_{1-x}Te_x$, the local structure of the $FeS_{1-x}Te_x$ ternary also shows a similar nature at the local scale. For example, the Fe–S and Fe–Te bond lengths in the ternary $FeS_{1-x}Te_x$ are close to the respective binaries (the Fe–S bond turns out to be almost 0.4 Å shorter

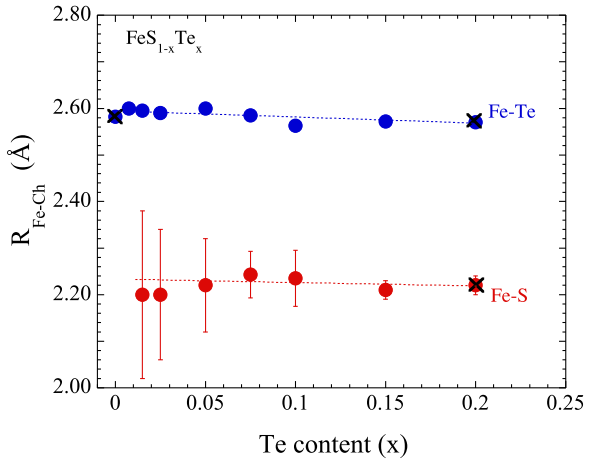


**Figure 6.** Fe–S and Fe–Te distances in $FeS_{1-x}Te_x$ as a function of Te concentration measured by high-resolution single-crystal x-ray diffraction [55]. The crossed symbols correspond to the distances measured by EXAFS analysis [29].

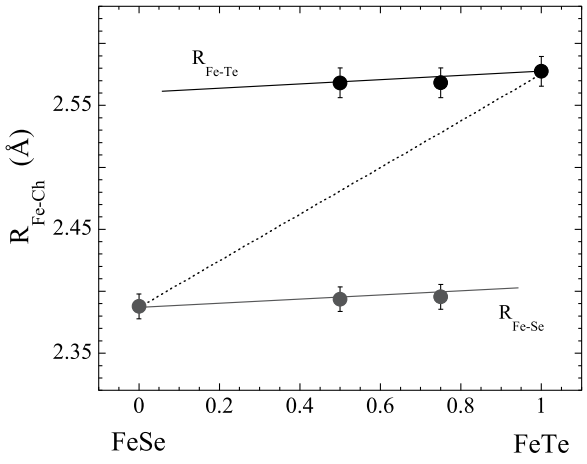


**Figure 7.** Fe–Se and Fe–Te distances determined by EXAFS and the average Fe–Ch distance (dashed line) as a function of concentration at low temperature showing the characteristic $Z$-plot of random alloys [29]. The dashed line is the average Fe–Ch distance, consistent with the diffraction measurements.

than the Fe–Te), observed by high-resolution neutron and single-crystal x-ray diffraction measurements on a series of $FeS_{1-x}Te_x$ [55]. Also, the EXAFS results are found to be consistent, revealing distinct Fe–S and Fe–Te distances in the ternary $FeS_{0.2}Te_{0.8}$ system. In fact, the Fe–S distance is ∼2.22 Å, close to the known distance (∼2.23 Å) in the FeS binary system [56]. We have shown the Fe–S and Fe–Te bond lengths on the $FeS_{1-x}Te_x$ system as a function of Te concentration measured by neutron and single-crystal x-ray diffraction [55] along with the EXAFS results in figure 6. Therefore, the local symmetry in the ternary chalcogenides with 11-type structure is broken in the crystallographically homogeneous system. This is different from the average structure measurements, showing a continuous evolution of the mean Fe–Ch distance as a function of the Te substitution. The mean Fe–Ch distances (weighted average) measured by the EXAFS are consistent with the average bond lengths measured by diffraction (figure 4); however, the local and average structures are different for the ternary chalcogenides.

The observed local structure diverging from the average structure in the $FeSe_{1-x}Te_x$ and $FeS_{1-x}Te_x$ ternary systems reminds us of random alloys. Indeed, the situation is similar to random alloys of the type $AB_{1-x}C_x$ in which local structure around the A site is not homogeneous although the end members AB and AC possess perfect crystallographic symmetry [57–61]. Indeed, the bond lengths A–B and A–C are non-equivalent and hence the bond angles are also so. These local distortions in the random alloys generally do not lead to new diffraction peaks, and could be explained by random distribution, reflecting lower symmetry of the crystal associated with the strain-relaxation arrangement of atomic sites. For an immediate comparison with the random alloys, the nearest-neighbor local Fe–Se and Fe–Te distances in the $FeSe_{1-x}Te_x$ ternary system are plotted as a function of Te concentration in figure 7. The behavior is similar to the so-called $Z$-plot, characteristic of the nearest-neighbor distances in ternary alloys [57–61]. It is clear that the local Fe–Se and Fe–Te bond lengths are closer to those in the binary end members (FeSe and FeTe) than what one expects from the prediction of Vegard's law [49]. Within the experimental uncertainties the bond lengths appear to remain unchanged in the case of the 11-system, albeit tending to increase with Te concentration; this is likely due to strain-relaxation atomic distribution in the inhomogeneous phase [49].

Various models have been discussed to describe the atomic-scale structure of the $AB_{1-x}C_x$ random alloys [62–65]. These studies have predicted the first nearest-neighbor distance between the A and C atoms ($d_{AC}$) in the dilute limit of an impurity atom C in a crystal AB ($d_{AC}^{AB:C}$). The dimensionless relaxation parameter $\epsilon$ is defined as the difference between $d_{AC}^{AB:C}$ and the (unperturbed) first nearest-neighbor distance of the host $d_{AB}^0$ relative to the difference in first nearest-neighbor distances of the two binaries, i.e. $\epsilon = (d_{AC}^{AB:C} - d_{AB}^0)/(d_{AC}^0 - d_{AB}^0)$. In the Pauling limit [49], in which the atomic radii are approximately conserved in different environments, the two bonds will be composition independent and equal to their ideal values $d_{AB}^0$ and $d_{AC}^0$, and hence $\epsilon = 1$ (full relaxation). On the other hand, Vegard's limit [49] corresponds to $\epsilon = 0$ (no relaxation) in which the alloy is thought to be sustaining a single (average) chemical bond (i.e. no bond alteration). In the case of $FeSe_{1-x}Te_x$, $\epsilon$ is ∼0.95, indicating a large average bond relaxation, unlike a large part of pseudobinary semiconductor alloys in which the relaxation parameter $\epsilon$ is ∼0.8 [57–61]. This could be due to (i) stronger Fe d–Ch p hybridization and (ii) larger order in the $FeSe_{1-x}Te_x$ chalcogenides compared to the pseudobinary semiconductor alloys [63, 64].

Since it is known that the chalcogen height from the Fe-plane ($h_z$) has a direct effect on the electronic properties of the Fe-based superconductors [13–15] and since the different chalcogen atoms (Se/S and Te) occupy distinct sites in the $FeSe_{1-x}Te_x$, there are different corresponding $h_z$. The Fermi surface topology strongly depends on the $h_z$ [13–15]; thus the configurationally inhomogeneous distribution of Se/S and Te atoms should have an obvious effect on the physical properties of $Fe(Se,S)_{1-x}Te_x$ ternary systems, behaving similarly to

ternary random alloys. However, the question is whether random alloys have a band structure and hence a Fermi surface. The answer is that the random alloys ($AB_{1-x}C_x$) do have a band structure (the so-called effective band structure containing contributions from the homogeneous parent AB and AC alloys). Incidentally, the alloying effect has hardly any influence on the effective band structure around the zone center [66], and the main effect of the alloying is away from the zone center. Indeed, angle resolved photoemission (ARPES) studies on the $FeSe_{1-x}Te_x$ systems [67, 68] have shown features similar to those expected in the random alloys. Among others, Tamai *et al* [68] have estimated a large effective electron mass and strong local electronic correlations in the $FeSe_{1-x}Te_x$ ternary system, which appears to be an apparent effect of alloying as in the case of random alloys. On the other hand, a careful ARPES has shown [69, 70] that the inhomogeneous electronic band structure is indeed a result of the random alloy-like local structure of these 11-type superconductors. It is fair to recall that the superconductivity in 11-type materials is very sensitive to the strain effects. FeTe is non-superconducting; however, it becomes superconducting under tensile strain with a $T_c$ as high as 13 K [71]. On the other hand, FeSe is superconducting with a $T_c$ of about 8 K which can be increased up to 37 K under hydrostatic pressure [72–74]. In addition, recent studies on $FeSe_{1-x}Te_x$ have shown that annealing the samples gives rise to a substantial increase in transition temperature in the ternary systems, with the superconductivity appearing in FeTe in the presence of very low Se contents [75]. We think that, while the higher $T_c$ in the ternary system should be due to strain relaxation, the increased $T_c$ in the annealed samples is merely due to higher local order, and hence further relaxation as expected in the random alloys [63, 64].

To summarize, local structure of $Fe(Se,S)_{1-x}Te_x$ (11-type) chalcogenides has been reviewed. The local structural studies have shown that Fe–Se/S and Fe–Te distances in the ternary $Fe(Se,S)_{1-x}Te_x$ are similar to the respective distances in the binary systems, consistent with significant divergence of the local structure from the average. The features observed in the local structural studies are characteristic of ternary random alloys, suggesting breaking of local symmetry in the 11-system in the absence a spacer layer.

### *3.2. Local disorder in the $K_{0.8}Fe_{1.6}Se_2$ chalcogenide: glass-like local structure*

Having discussed the nature of the local structure of 11-type chalcogenides that have no spacer layer, showing random alloy-like local symmetry breaking, let us turn to another chalcogenide in which the FeSe layers are intercalated (figure 1). It is known that the superconducting transition temperature of FeSe shows a large enhancement of up to ∼37 K under hydrostatic pressure [73, 74]. The large pressure sensitivity of FeSe indicates that chemical pressure is a potential alternative parameter for raising its $T_c$. Indeed, superconductivity at a $T_c$ as high as 32 K is known to appear in a K-intercalated FeSe [11], which has triggered new

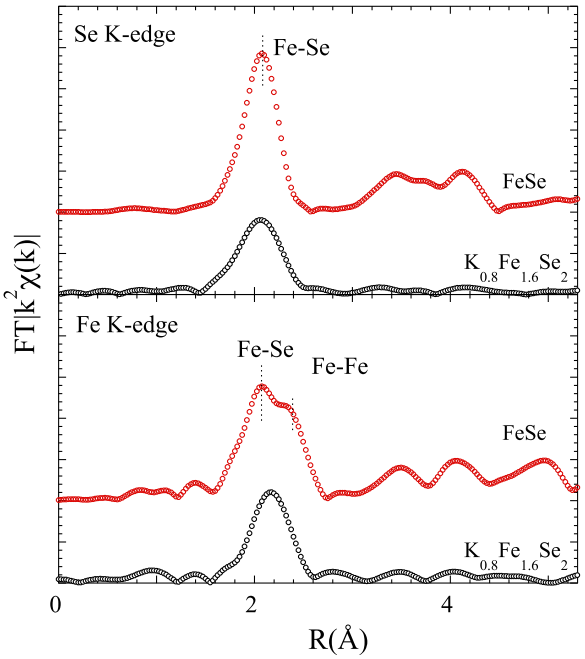


**Figure 8.** Comparison between local structures of FeSe (11-type structure) and $K_{0.8}Fe_{1.6}Se_2$ (122-type structure). FT magnitudes of the Fe K and Se *K*-edge EXAFS are shown at $T = 80$ K.

studies on the iron-based chalcogenides. A similar $T_c$ was observed in the $Rb_xFe_{2-y}Se_2$ [76, 77], $(Tl,K)Fe_{2-y}Se_2$ [78] and $Cs_xFe_{2-y}Se_2$ compounds [79]. Although isostructural to the 122-type pnictides (figure 1), $K_xFe_{2-y}Se_2$ has a distinct microstructure, characterized by an iron-vacancy order and a phase separation [80–84]. The magnetic order co-exists with a bulk superconductivity and a remarkably large iron magnetic moment [93–95]. These 122-type chalcogenides not only show superconductivity at temperatures comparable to those of the pnictides, but also reveal insulating and magnetic properties at several compositions, establishing a closer link to the cuprates. In addition, these 122-type chalcogenides have no hole pockets in the Fermi surface [85–87], and hence do not favor the widely discussed ideas based on the nesting between electron pockets and hole pockets. There are also experimental indications of the relation between superconductivity and iron-vacancy disorder, with a completely ordered state being an insulator. For the general properties of 122-chalcogenides, see the recent review by Dagotto [88]. Here, we have review briefly the local structure of $K_{0.8}Fe_{1.6}Se_2$ system, which is characterized by a large disorder similar to the amorphous/glass materials.

Let us start by discussing differences in the local structure of the intercalated FeSe, i.e. $K_{0.8}Fe_{1.6}Se_2$, and the pristine binary FeSe. Figure 8 compares FTs of the Fe and Se *K*-edge EXAFS signals on the FeSe sample [26] and the $K_{0.8}Fe_{1.6}Se_2$. The Fe nearest neighbors in FeSe are Se at a distance of ∼2.4 Å and Fe atoms at a distance of ∼2.7 Å (two-peak structure at ∼1.5–3.0 Å), similar to the case of $K_{0.8}Fe_{1.6}Se_2$. Similarly, in the Se *K*-edge EXAFS of FeSe we expect a contribution from four Fe nearest neighbors at a distance of ∼2.4 Å (as in the $K_{0.8}Fe_{1.6}Se_2$). The contribution of distant shells appears as a multiple structured peak at ∼3.0–4.5 Å.

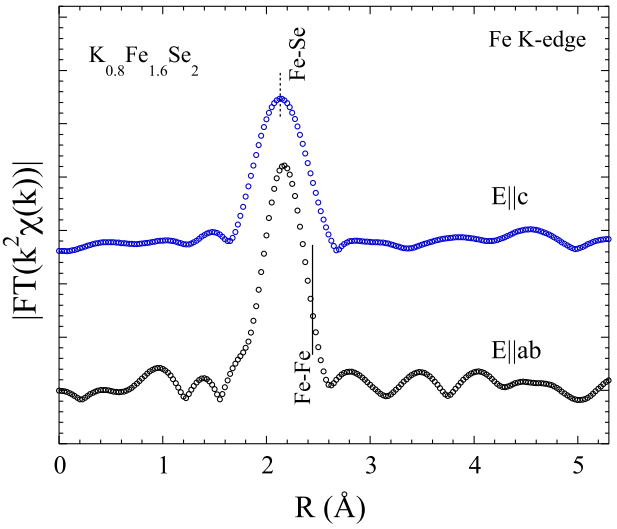


**Figure 9.** FT magnitudes of the polarized Fe *K*-edge EXAFS (weighted by $k^2$) on $K_{0.8}Fe_{1.6}Se_2$ single crystals [31].

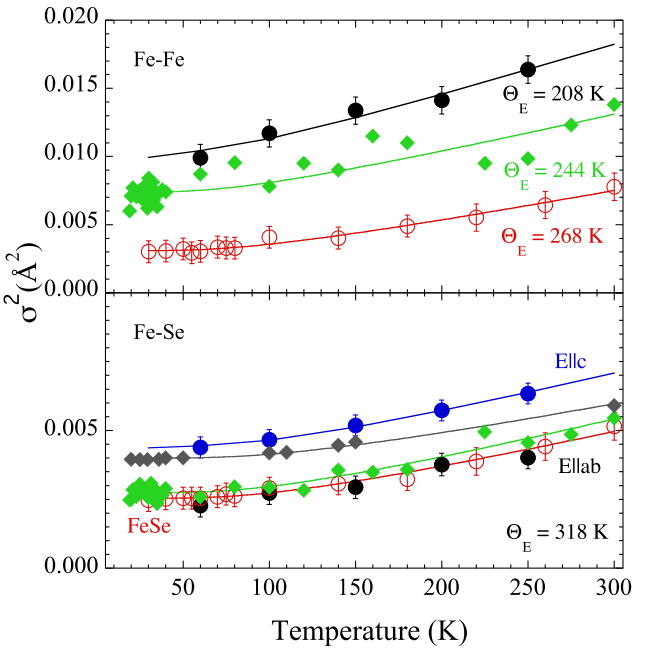


**Figure 10.** Fe–Se and Fe–Fe MSRDs (symbols) for the $K_{0.8}Fe_{1.6}Se_2$ system taken from different EXAFS studies are compared with the case of binary FeSe (11-structure). The red symbols represent the data for the binary FeSe system, while the black [31], blue [31], green [33] and gray [34] symbols are the data for the 122-chalcogenide.

The comparison underlines significant differences in the local structure of the FeSe and the $K_{0.8}Fe_{1.6}Se_2$ systems. In particular, the FT of the $K_{0.8}Fe_{1.6}Se_2$ shows only a single peak at ∼2 Å that contains the contribution from the Fe–Se distances (∼2.4 Å) in the Se *K*-edge EXAFS and Fe–Se and Fe–Fe contributions in the Fe *K*-edge EXAFS. The longer distance contributions are strongly suppressed and are apparently absent in the case of the $K_{0.8}Fe_{1.6}Se_2$ system. In addition, the contribution from the Fe–Fe distances in the Fe *K*-edge EXAFS is strongly damped, indicating a large Fe site disorder. Apparently, the EXAFS data reveal large overall local disorder in the $K_{0.8}Fe_{1.6}Se_2$ system, commonly seen in the local structure of amorphous systems [89]. On the other hand, the $K_{0.8}Fe_{1.6}Se_2$ sample used for these studies is a very good single crystal, evident from sharp diffraction peaks [83, 84], and such a large disorder in the local structure indicates that the $K_{0.8}Fe_{1.6}Se_2$ should be some kind of glassy system involving atomic structure.

Further clues to the nature of disorder can be obtained by comparing polarized EXAFS in different geometries. Figure 9 shows the FT magnitudes of Fe *K*-edge EXAFS measured on a $K_{0.8}Fe_{1.6}Se_2$ single-crystal sample in two polarization geometries. The FT magnitudes of the polarized EXAFS provide partial atomic distribution around the Fe in the direction of x-ray beam polarizations. The Fe site nearest neighbors are Se (at a distance of ∼2.4 Å) and Fe (at a distance of ∼2.7 Å) in the $E \parallel ab$ polarization. The contribution of the Fe–Fe is not expected in the $E \parallel c$ polarization and the main FT peak in this geometry should be merely due to Fe–Se bonds. Contributions of Fe next nearest neighbors are expected to appear at longer distances ($R_{Fe-Fe} = 3.91$ Å, $R_{Fe-K} = 4.02$ Å and $R_{Fe-Se} = 4.62$ Å). Therefore, the main FT peak of the Fe *K*-edge EXAFS in the $E \parallel ab$ geometry contains information on the Fe–Se and Fe–Fe bonds, while that in the $E \parallel c$ has a contribution only of Fe–Se bonds, similar to the main FT peak of the Se *K*-edge EXAFS (figure 8). As underlined in figure 8, the contributions expected from the farther atoms are apparently absent, which is a characteristic feature of highly disordered systems and amorphous materials [89]. In addition, the Fe–Se distances determined by EXAFS in different polarizations on two edges are similar [30] within experimental uncertainties; however, both Fe–Se and Fe–Fe distances are slightly shorter than the average bond lengths determined by diffraction studies [80–84, 90]. This seems to be the case mainly due to largely disordered atomic structure, similar to glassy systems [91, 92].

Incidentally, the Fe–Se bond lengths hardly show any change with temperature unlike the Fe–Fe distance (describing the in-plane lattice parameter) that varies with temperature showing relative flexibility of the latter. This has been seen by different EXAFS studies on the 122-type chalcogenide system [31, 33, 34]. Indeed, EXAFS permits one to obtain information on bond length flexibility through temperature-dependent Debye–Waller factors of the bond lengths. Figure 10 shows the correlated DWFs ($\sigma^2$), i.e. the MSRDs of the Fe–Se and the Fe–Fe pairs plotted as a function of temperature for the $K_{0.8}Fe_{1.6}Se_2$, compared with the $\sigma^2$ of the two bond lengths for the binary FeSe system [26]. The data on the Fe–Se bond length are taken from three different EXAFS studies [31, 33, 34] while those on Fe–Fe bond lengths are taken from two different studies [31, 33] on the $K_{0.8}Fe_{1.6}Se_2$ system.

As discussed earlier, the $\sigma^2$ measured by EXAFS (represents distance broadening) is the sum of temperature-independent ($\sigma_0^2$) and temperature-dependent terms, i.e. $\sigma^2 = \sigma_0^2 + \sigma^2(T)$. The temperature-dependent part can be described by the correlated Eisntein model (see, e.g., section 2). The Einstein temperature ($\theta_E$, i.e. the Einstein

frequency $\omega_E = k_B\theta_E/\hbar$) for the Fe–Se pairs determined in different EXAFS studies is similar. For example, Iadecola *et al* [31] found that $\theta_E \sim 318$ K, similar to that in the binary FeSe system, indicating that the force constant ($k = \mu\omega_E^2$, where $k$ is the effective force constant and $\mu$ is the reduced mass of the Fe–Se pair) of the Fe–Se bond lengths is not very sensitive to the K-intercalation between the FeSe layers. The estimated force constant for the Fe–Se bond length is $k \sim 5.8$ eV Å$^{-2}$. The EXAFS study by Tyson *et al* [33] also found a similar $\theta_E$ (~308 K) for the Fe–Se bond length, incidentally similar to the case of Fe–As bond length in the 1111-type structure. The $\theta_E$ estimated by Ryu *et al* [34] is slightly higher ($\theta_E \sim 353$ K) than the other two studies; however, it should be noted that the result is based on limited temperature points at higher temperature (their study reports just one temperature point above 150 K).

While the Fe–Se force constant remains almost similar to that in 11-type chalcogenide, there is a substantial effect of intercalation on the Einstein temperature (force constant) of the Fe–Fe pairs, estimated to be ~208 K ($k \sim 2.1$ eV Å$^{-2}$) and ~268 K ($k \sim 3.5$ eV Å$^{-2}$), for $K_{0.8}Fe_{1.6}Se_2$ and the binary FeSe, respectively [31]. Therefore, it appears that the Fe–Fe bond lengths are relatively relaxed in $K_{0.8}Fe_{1.6}Se_2$, consistent with the glassy nature of this system. The results are consistent with other EXAFS studies [33] revealing that $\theta_E$ for the Fe–Fe bond length is ~244 K, lower than the $\theta_E$ in 11-type chalcogenides and 1111-type oxypnictides. It should be mentioned that all the local structure studies find large local disorder in 122-type chalcogenides [31, 33, 34].

The temperature-independent term of the EXAFS DWF ($\sigma_0^2$) is mainly given by the static configurational disorder. The $\sigma_0^2$ (~0.0002) for the Fe–Se pairs in $E \parallel ab$ polarization is small (figure 10) and is approximately similar to that for the binary FeSe (for similar $k$-resolutions in the two systems). On the other hand, the $\sigma_0^2$ for the $E \parallel c$ is relatively large (~0.002). This difference in the $\sigma_0^2$ along the two polarizations clearly points out a larger static disorder being along the $c$-direction, likely to be due to the $K$-intercalation. It should be noted that the differences in $\sigma_0^2$ between different EXAFS studies are due to different $k$-resolutions. Tyson *et al* [33] have measured K $K$-edge EXAFS and provided direct information on the local structure around the intercalated K atoms. Figure 11 shows the FT of K $K$-edge EXAFS measured on the $K_{0.8}Fe_{1.6+x}Se_2$ system along with the FT of the calculated EXAFS spectrum considering the average crystallographic structure. It is clear that the signal due to K–Se distance is strongly damped with respect to what is expected from an average structure. This indicates a large disorder in the $K$-layers. The K $K$-edge EXAFS data are consistent with Fe $K$-edge and Se $K$-edge EXAFS data (figure 8) in which the signals due to Fe–K and Se–K distances are hardly seen.

It should be mentioned that the $\sigma_0^2$ for the Fe–Fe is substantially large, a mere indicator of Fe site configurational disorder. Considering that the system has a well-defined crystalline ordering, the glassy local structure could be due to freezing of the iron-vacancy order coupled with disorder of some other degrees of freedom, such as the

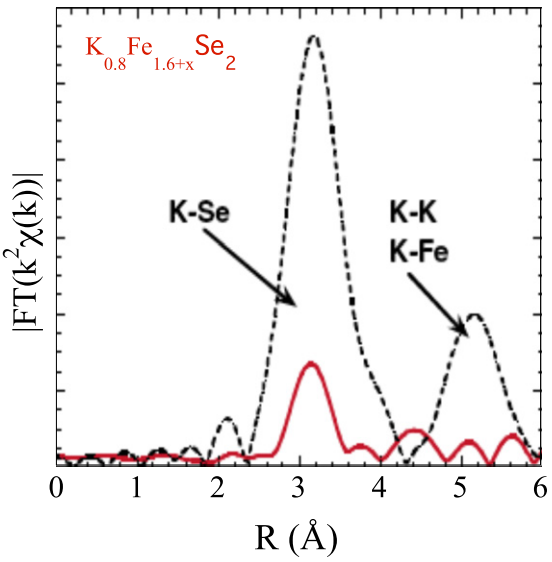


**Figure 11.** FT magnitudes of K $K$-edge EXAFS (weighted by $k^2$) on the $K_{0.8}Fe_{1.6+x}Se_2$ system [33].

$K$-layer disorder. Several measurements have undelined that the magnetic ordering in this system co-exists with the superconductivity with a large iron moment (3.3 $\mu_B$/Fe) ordered antiferromagnetically along the $c$-axis [93–95]. Local structure measurements using EXAFS [31, 33] reveal that there is (i) a large static disorder along the $c$-axis, (ii) a large disorder in the $K$-layer and (iii) a large Fe-site disorder. In addition, the Fe–Fe bond length (in-plane lattice parameter) is relatively relaxed. Therefore, it appears plausible to think that a frozen state comprising $c$-axis disorder (associated with local strain fields due to $K$-intercalation and iron–vacancy order) coupled with magnetic order is realized. This frozen state could result in magnetic textures with large frozen magnetic moment and a relaxed Fe–Fe network. Thus, it is likely that the strain fields locally compress the FeSe block and hence the $T_c$ reaches a value as high as 32 K, as happens for FeSe under external pressure. Indeed, single-crystal x-ray diffraction has shown clear evidence for nanoscale phase separation between a majority magnetic phase with iron-vacancy ordering, co-existing with a minority compressed phase [83, 84]. The phase separation corresponds to the electronic phase separation, also revealed by high-energy spectroscopy [96] showing different phases characterized by different Fe-spin states. This situation is similar to granular superconductors in which a nanoscale superconducting phase coexists within an insulating texture. Therefore, the physics of the 122-type chalcogenide system should be quite similar to the physics of glasses and granular superconductors. It should be recalled that the thermodynamic and kinetic fragility of a glass is related to the number of potential energy minima in the phase space and the heights of the activation energy barriers separating these minima. Another fact that supports that the superconductivity in the $K_{0.8}Fe_{1.6}Se_2$ system depends strongly on its thermal history [97] is the characteristic feature of glasses.

In summary, local structure studies on 122-type chalcogenide reveal that the system is characterized by

disordered materials-like local structure, indicating glassy nature of these materials. The glassy nature is driven by large static disorder in the $c$-axis, likely to be due to configurational disorder in the intercalated K-layer. In addition, the Fe–Fe force constant turns out to be smaller than the simple 11-type binary FeSe system. Such a local relaxation of the Fe–Fe bond length is due to a compression of the FeSe unit, as happens under external pressure, and hence the superconductivity at high $T_c$ in the $K_{0.8}Fe_{1.6}Se_2$ system should be due to a locally compressed nanoscale minority phase, co-existing with the normal magnetic phase, similar to granular superconductors.

## 4. Conclusions

We have reviewed studies of the local structure in 11-type and 122-type chalcogenides. While the 11-type structure does not have the spacer layer, the 122-structure has intercalated alkaline atoms instead of a spacer layer. The local structure clearly underlines the fact that in the absence of a spacer layer the structure is highly susceptible to topological changes. Indeed, when a chalcogen atom in the 11-structure is partially substituted, the local symmetry of the structure suffers a breakdown with nanoscale phase separation characterized by co-existing different Fe–Ch bond lengths. This is similar to the case of semiconductor random alloys having a direct influence on the fundamental electronic structure. The fact that the chalcogen height from the Fe-plane ($h_z$) has a direct effect on the electronic properties of the Fe-based superconductors [13–15], and since the chalcogen atoms (Se or S and Te) occupy distinct sites in the $Fe(Se,S)_{1-x}Te_x$, there are different corresponding $h_z$. The Fermi surface topology strongly depends on the $h_z$ [13–15]; thus the configurationally inhomogeneous distribution of Ch atoms should have an obvious effect on the physical properties of $FeSe_{1-x}Te_x$ ternary systems, behaving similarly to ternary random alloys.

The case of the $K_{0.8}Fe_{1.6}Se_2$ system is very interesting due to its unusual microstructure having direct implications for the fundamental electronic structure. One of these features is the absence of hole pockets on the Fermi surface, differentiating the system from other iron-based superconductors, including the isostructural 122-type pnictides. This has a direct influence on the widely discussed Fermi surface nesting picture of these materials. Also, the coexisting insulating phase with iron-vacancy order and antiferromagnetism are other important features of 122-type chalcogenides. In addition, the presence of an exotic phase separation in this system is now well established, which ranges from nanoscale to microscale. The role of this phase separation is still under debate and more and more studies are coming up to compare these materials with the exotic phase of high-$T_c$ copper oxides and other transition metal oxides such as manganites. While the 11-type structure suffers local symmetry breakdown due to the absence of a spacer layer to compensate for the effects of any external fields (e.g. the strain fields due to substitution), a glass-like local disorder appears when the 11-layers are intercalated (e.g. the case of 122-type chalcogenides). The observation of a glassy nature puts the system in the category of granular superconductors, consistent with the superconductivity in A15 systems [98] and the recently observed fractal distribution enhanced superconductivity in superoxygenated $La_2CuO_4$ [99, 100].

These features of the local structure of iron-based chalcogenides are different from the local structure of 1111-type iron-based pnictide structures. Indeed, 1111-type structures have a well-defined spacer layer and the structure is less susceptible to external fields such as the strain effects due to chemical pressure or the charge density introduced through substitutions or defects. In fact, local structure studies on the 1111-type materials [22–25, 31] have shown that the interlayer atomic correlations play an important role in local structural displacements controlling the stability of the structure, unlike the 11-type and 122-type chalcogenides. The local structure studies discussed here underline the importance of the structural topology and local chemistry with the glassy nature of these complex phases being key to the exotic properties of these new superconductors.

## Acknowledgments

The author thanks A Iadecola, B Joseph, Y Mizuguchi, A Puri, L Simonelli, Y Takano, M Takeya for their fruitful collaboration in this work. Thanks are also due to A Bianconi and T Mizokawa for useful discussions.

## References

[1] Kamihara Y, Watanabe T, Hirano M and Hosono H 2008 *J. Am. Chem. Soc.* **130** 3296
[2] Ishida K, Nakai Y and Hosono H 2009 *J. Phys. Soc. Japan* **78** 062001
[3] Ren Z A and Zhao Z X 2009 *Adv. Mater.* **21** 4584
[4] Johnston D C 2010 *Adv. Phys.* **59** 803
[5] Stewart G R 2011 *Rev. Mod. Phys.* **83** 1589
[6] Hsu F C *et al* 2008 *Proc. Natl Acad. Sci. USA* **105** 14262
[7] Mizuguchi Y and Takano Y 2010 *J. Phys. Soc. Japan* **79** 102001
[8] Wen J, Xu G, Gu G, Tranquada J M and Birgeneau R J 2011 *Rep. Prog. Phys.* **74** 124503
[9] Deguchi K, Takano Y and Mizuguchi Y 2012 arXiv:1210.1305
[10] Ogino H, Shimizu Y, Kawaguchi N, Kishio K, Shimoyama J, Tohei T and Ikuhara Y 2011 *Supercond. Sci. Technol.* **24** 085020
[11] Guo J, Jin S, Wang G, Wang S, Zhu K, Zhou T, He M and Chen X 2010 *Phys. Rev.* B **82** 180520
[12] Andersen O K and Boeri L 2011 *Ann. Phys., Lpz.* **523**(1) 8
[13] Subedi A, Zhang L, Singh D J and Du M H 2008 *Phys. Rev.* B **78** 134514
[14] Miyake T, Nakamura K, Arita R and Imada M 2010 *J. Phys. Soc. Japan* **79** 044705
[15] Moon C Y and Choi H J 2010 *Phys. Rev. Lett.* **104** 057003
[16] Sefat A S 2011 *Rep. Prog. Phys.* **74** 124502
[17] Mizuguchi Y, Hara Y, Deguchi K, Tsuda S, Yamaguchi T, Takeda K, Kotegawa H, Tou H and Takano Y 2010 *Supercond. Sci. Technol.* **23** 054013
[18] Lee C H, Iyo A, Eisaki H, Kito H, Fernandez-Diaz T M, Ito T, Kihou K, Matsuhata H, Braden M and Yamada K 2008 *J. Phys. Soc. Japan* **77** 083704
[19] Louca D *et al* 2010 *Phys. Rev.* B **81** 134524
[20] Hu R, Bozin E S, Warren J B and Petrovic C 2009 *Phys. Rev.* B **80** 214514

[21] Zhang C J, Oyanagi H, Sun Z H, Kamihara Y and Hosono H 2010 *Phys. Rev.* B **81** 094516
[22] Iadecola A, Agrestini S, Filippi M, Simonelli L, Fratini M, Joseph B, Mahajan D and Saini N L 2009 *Europhys. Lett.* **87** 26005
[23] Joseph B, Iadecola A, Fratini M, Bianconi A, Marcelli A and Saini N L 2009 *J. Phys.: Condens. Matter* **21** 432201
[24] Xu W, Marcelli A, Joseph B, Iadecola A, Chu W S, Di Gioacchino D, Bianconi A, Wu Z Y and Saini N L 2010 *J. Phys.: Condens. Matter* **22** 125701
[25] Xu W, Joseph B, Iadecola A, Marcelli A, Chu W S, Di Gioacchino D, Bianconi A, Wu Z Y and Saini N L 2010 *Europhys. Lett.* **90** 57001
[26] Joseph B, Iadecola A, Puri A, Simonelli L, Mizuguchi Y, Takano Y and Saini N L 2010 *Phys. Rev.* B **82** 020502
[27] Iadecola A, Joseph B, Simonelli L, Mizuguchi Y, Takano Y and Saini N L 2010 *Europhys. Lett.* **90** 67008
[28] Joseph B, Iadecola A, Malavasi L and Saini N L 2011 *J. Phys.: Condens. Matter* **23** 265701
[29] Iadecola A, Joseph B, Puri A, Simonelli L, Mizuguchi Y, Testemale D, Proux O, Hazemann J L, Takano Y and Saini N L 2011 *J. Phys.: Condens. Matter* **23** 425701
[30] Iadecola A, Joseph B, Simonelli L, Puri A, Mizuguchi Y, Takeya H, Takano Y and Saini N L 2012 *J. Phys.: Condens. Matter* **24** 115701
[31] Iadecola A, Joseph B, Simonelli L, Maugeri L, Fratini M, Martinelli A, Palenzona A, Putti M and Saini N L 2012 *Phys. Rev.* B **85** 214530
[32] Cheng J *et al* 2011 *J. Synchrotron Radiat.* **18** 723
[33] Tyson T A, Yu T, Han S J, Croft M, Gu G D, Dimitrov I K and Li Q 2012 *Phys. Rev.* B **85** 024504
[34] Ryu H, Lei H, Frenkel A I and Petrovic C 2012 *Phys. Rev.* B **85** 224515
[35] Egami T and Billinge S J L (ed) 2003 *Underneath the Bragg Peaks: Structural Analysis of Complex Materials* (*Pergamon Materials Series* vol 7) (UK: Pergamon/ Elsevier)
[36] Prinz R and Koningsberger D J (ed) 1988 *X-Ray Absorption: Principle Applications Techniques of EXAFS SEXAFS and XANES* (New York: Wiley)
[37] Bozin E S, Kwei G H, Takagi H and Billinge S J L 2000 *Phys. Rev. Lett.* **84** 5856 and references therein
[38] McQueeney R J, Petrov Y, Egami T, Yethiraj M, Shirane G and Endoh Y 1999 *Phys. Rev. Lett.* **82** 628
[39] McQueeney R J, Sarrao J L, Pagliuso P G, Stephens P W and Osborn R 2001 *Phys. Rev. Lett.* **87** 077001
[40] Saini N L, Bianconi A and Oyanagi H 2001 *J. Phys. Soc. Japan* **70** 2092
[41] Saini N L, Oyanagi H, Ito T, Scagnoli V, Filippi M, Agrestini S, Campi G, Oka K and Bianconi A 2003 *Eur. Phys. J.* B **36** 75
[42] Saini N L, Oyanagi H, Ito T, Scagnoli V, Ito T, Oka K and Bianconi A 2003 *J. Phys. Soc. Japan* **72** 829
[43] Saini N L, Oyanagi H, Ito T, Scagnoli V, Ito T, Oka K and Bianconi A 2003 *Europhys. Lett.* **63** 125
[44] Bianconi A, Saini N L, Lanzara A, Missori M, Rossetti T, Oyanagi H, Yamaguchi H, Oka K and Ito T 1996 *Phys. Rev. Lett.* **76** 3412
[45] Saini N L, Lanzara A, Oyanagi H, Yamaguchi H, Oka K, Ito T and Bianconi A 1997 *Phys. Rev.* B **55** 12759
[46] Saini N L, Lanzara A, Bianconi A, Oyanagi H, Yamaguchi H, Oka K and Ito T 1996 *Physica* C **268** 121
[47] Sevillano E, Meuth H and Rehr J J 1979 *Phys. Rev.* B **20** 4908
[48] See e.g. a review by Rehr J J and Albers R C 2000 *Rev. Mod. Phys.* **72** 621
[49] See e.g. Deb S K and Zunger A (ed) 1987 *Ternary and Multinary Compounds* (Pittsburg: Materials Research Society)
[50] Horigane K, Hiraka H and Ohoyama K 2009 *J. Phys. Soc. Japan* **78** 074718
[51] McQueen T M, Williams A J, Stephens P W, Tao J, Zhu Y, Ksenofontov V, Casper F, Felser C and Cava R J 2009 *Phys. Rev. Lett.* **103** 057002
[52] Mustre de Leon J, Rehr J J, Zabinsky S I and Albers R C 1991 *Phys. Rev.* B **44** 4146
[53] Hu H, Zuo J M, Wen J, Xu Z, Lin Z, Li Q, Gu G, Park W K and Greene L H 2011 *New J. Phys.* **13** 053031
[54] He X, Li G, Zhang J, Karki A B, Jin R, Sales B C, Sefat A S, McGuire M A, Mandrus D and Plummer E W 2011 *Phys. Rev.* B **83** 220502
[55] Zajdel P, Hsieh P Y, Rodriguez E E, Butch N P, Magill J D, Paglione J, Zavalij P, Suchomel M R and Green M A 2010 *J. Am. Chem. Soc.* **132** 13000
[56] See e.g. O'Day P A, Rivera N Jr, Root R and Carroll S A 2004 *Am. Mineral.* **89** 572
[57] Mikkelsen J C Jr and Boyce J B 1982 *Phys. Rev. Lett.* **49** 1412
[58] Balzarotti A, Czyzyk M, Kisiel A, Motta N, Podgrny M and Zimnal-Starnawska M 1984 *Phys. Rev.* B **30** 2295
[59] Islam Q T and Bunker B A 1987 *Phys. Rev. Lett.* **59** 2701
[60] Happo N, Sato H, Mihara T, Mimura K, Hosokawa S, Ueda Y and Taniguchi M 1996 *J. Phys.: Condens. Matter* **8** 4315
[61] Peterson P F, Proffen T, Jeong I K, Billinge S J L, Choi K S, Kanatzidis M G and Radaelli P G 2001 *Phys. Rev.* B **63** 165211
[62] Martins J L and Zunger A 1984 *Phys. Rev.* B **30** 6217
[63] Zunger A 1987 *Appl. Phys. Lett.* **50** 164
[64] Srivastava G P, Martins J L and Zunger A 1985 *Phys. Rev.* B **31** 2561
[65] Duan H, Chen X, Huang Y, Zhou X, Sun L and Lu W 2007 *Phys. Rev.* B **76** 035209
[66] Popescu V and Zunger A 2010 *Phys. Rev. Lett.* **104** 236403
[67] Xia Y, Qian D, Wray L, Hsieh D, Chen G F, Luo J L, Wang N L and Hasan M Z 2009 *Phys. Rev. Lett.* **103** 037002
[68] Tamai A *et al* 2010 *Phys. Rev. Lett.* **104** 097002
[69] Mizokawa T *et al* 2012 *J. Supercond. Novel Magn.* **25** 1343
[70] Sudayama T, Wakisaka Y, Ootsuki D, Mizokawa T, Saini N L, Arita M, Namatame H, Taniguchi M, Noji T and Koike Y 2012 arXiv:1206.3917
[71] Han Y, Li W Y, Cao L X, Wang X Y, Xu B, Zhao B R, Guo Y Q and Yang J L 2010 *Phys. Rev. Lett.* **104** 017003
[72] Margadonna S, Takabayashi Y, McDonald M T, Kasperkiewicz K, Mizuguchi Y, Takano Y, Fitch A N, Suard E and Prassides K 2008 *Chem. Commun.* 5607
[73] Mizuguchi Y, Tomioka F, Tsuda S, Yamaguchi T and Takano Y 2008 *Appl. Phys. Lett.* **93** 152505
[74] Medvedev S *et al* 2009 *Nature Mater.* **8** 630
[75] Noji T, Suzuki T, Abe H, Adachi T, Kato M and Koike Y 2010 *J. Phy. Soc. Japan* **79** 084711
[76] Wang A F *et al* 2011 *Phys. Rev.* B **83** 060512
[77] Li C H, Shen B, Han F, Zhu X and Wen H H 2011 *Phys. Rev.* B **83** 184521
[78] Fang M, Wang H, Dong C, Li Z, Feng C, Chen J and Yuan H Q 2011 *Europhys. Lett.* **94** 27009
[79] Ying J J *et al* 2011 *Phys. Rev.* B **83** 212502
[80] Ye F, Chi S, Bao W, Wang X F, Ying J J, Chen X H, Wang H D, Dong C H and Fang M 2011 *Phys. Rev. Lett.* **107** 137003
[81] Zavalij P *et al* 2011 *Phys. Rev.* B **83** 132509
[82] Wang Z, Song Y J, Shi H L, Wang Z W, Chen Z, Tian H F, Chen G F, Guo J G, Yang H X and Li J Q 2011 *Phys. Rev.* B **83** 140505
[83] Ricci A *et al* 2011 *Supercond. Sci. Technol.* **24** 082002
[84] Ricci A *et al* 2011 *Phys. Rev.* B **84** 060511
[85] Zhang Y *et al* 2011 *Nature Mater.* **10** 273

[86] Richard P, Sato T, Nakayama K, Takahashi T and Ding H 2011 *Rep. Prog. Phys.* **74** 124512
[87] Qian T *et al* 2011 *Phys. Rev. Lett.* **106** 187001
[88] Dagotto E 2012 arXiv:1210.6501v1
[89] See e.g. a recent review on glasses by Greaves G N and Sen S 2007 *Adv. Phys.* **56** 1 and relevant references
[90] Bacsa J, Ganin A Y, Takabayashi Y, Christensen K E, Prassides K, Rosseinskya M J and Claridge J B 2011 *Chem. Sci.* **2** 1054
[91] Kolobov A V, Oyanagi H and Tanaka K 1997 *Phys. Rev.* B **55** 726
Kolobov A V, Oyanagi H and Tanaka K 2001 *Phys. Rev. Lett.* **87** 145502
[92] Majid M, Benazeth S, Souleau C and Purans J 1998 *Phys. Rev.* B **58** 6104
[93] Bao W, Huang Q, Chen G F, Green M A, Wang D M, He J B, Wang X Q and Qiu Y 2011 *Chinese Phys. Lett.* **28** 086104
[94] Pomjakushin V Y, Sheptyakov D V, Pomjakushina E V, Krzton-Maziopa A, Conder K, Chernyshov D, Svitlyk V and Shermadini Z 2011 *Phys. Rev.* B **83** 144410
[95] Pomjakushin V Y, Pomjakushina E V, Krzton-Maziopa A, Conder K and Shermadini Z 2011 *J. Phys.: Condens. Matter* **23** 156003
[96] Simonelli L, Saini N L, Moretti Sala M, Mizuguchi Y, Takano Y, Takeya H, Mizokawa T and Monaco G 2012 *Phys. Rev.* B **85** 224510
[97] Han F, Shen B, Wang Z Y and Wen H H 2011 arXiv:1103.1347v1
[98] Testardi L R 1975 *Rev. Mod. Phys.* **47** 637
[99] Fratini M, Poccia N, Ricci A, Campi G, Burghammer M, Aeppli G and Bianconi A 2010 *Nature* **466** 841
[100] Poccia N *et al* 2012 *Proc. Natl Acad. Sci. USA* **109** 15685